Asia-Pacific Journal of Sports Medicine, Arthroscopy, Rehabilitation and Technology 36 (2024) 28–39

Contents lists available at ScienceDirect

Asia-Pacific Journal of Sports Medicine, Arthroscopy, Rehabilitation and Technology

journal homepage: www.ap-smart.com

Original article

Histologic and biomechanical comparison of fascia lata autograft, acellular dermal xenograft, and synthetic patch for bridging massive rotator cuff tear in a rabbit model

Yuyan Na [1], Hao Jue [1], Tian Xia [1], Xiaoao Xue, Luyi Sun, Jun Chen [**], Yinghui Hua [*]

Department of Sports Medicine, Huashan Hospital, Fudan University, Shanghai, China

ARTICLE INFO

Keywords:
Acellular dermal matrix
Bridging repair
Fascia lata
Massive rotator cuff tears
PET

ABSTRACT

Background: Bridging repair has emerged as a promising and reliable treatment strategy for the massive rotator cuff tears (MRCTs). However, there remains a lack of evidence on which bridging graft provides the better repair results, and a dearth of animal studies comparing bridging repairs with different grafts. The purpose of this study was to evaluate the histological and biomechanical outcomes of commonly used grafts (autologous fascia lata (FL), acellular dermal matrix graft (ADM), and polyethylene terephthalate (PET) patch).

Methods: A total of 66 male New Zealand White Rabbits were used to mimic a model of unilateral chronic MRCTs. The rabbits were randomly divided into three groups: (1) FL group, which underwent bridging repair with autologous FL; (2) ADM group, which underwent bridging with ADM; and (3) PET group, which underwent bridging with PET patch. Tissue samples were collected and subjected to histological analysis using Hematoxylin and eosin, Picrosirius red, Safranin O/Fast green staining, and Immunostaining. Collagen diameter and fibril density in the regenerated tendon was analyzed with transmission electron microscopy (TEM). Additionally, biomechanical tests were performed at 6 and 12 weeks after repair.

Results: The regenerated tendon successfully reattached to the footprint in all experimental groups. At 6 weeks after repair, the FL group had a significantly higher Modified Tendon Histological Evaluation (MTHE) score at the regenerated tendon than the PET group (13.2 ± 1.64 vs 9.6 ± 1.95, respectively; $P = 0.038$). The picrosirius red staining results showed that the FL group had a significantly higher type I collagen content than the ADM and PET groups at 6 weeks, and this difference was sustained with the PET group at 12 weeks ($P < 0.05$). Immunofluorescence analysis against CD68 indicated that the number of macrophage infiltrates was significantly lower in the FL group than in the ADM and PET groups ($P < 0.05$). At 12 weeks after repair, the area of Safranin O metachromasia was significant greater in ADM group than that in the PET group ($P = 0.01$). The FL group showed a significantly larger collagen diameter in the regenerated tendon than the PET group ($P < 0.05$), as indicated by TEM results. Furthermore, the FL group resulted in a greater failure load (at 6 weeks; 118.40 ± 16.70 N vs 93.75 ± 9.06 N, respectively; $P = 0.019$) and elastic modulus (at 6 weeks; 12.28 ± 1.94 MPa vs 9.58 ± 0.79 MPa, respectively; $P = 0.024$; at 12 weeks; 15.02 ± 2.36 MPa vs 11.63 ± 1.20 MPa, respectively; $P = 0.032$) than the ADM group.

Conclusions: This study demonstrated that all three grafts could successfully bridging chronic MRCTs in a rabbit model. However, autologous FL promoted tendon regeneration and maturation, and enhanced the tensile properties of the tendon-to-bone complex when compared with ADM and PET grafts.

1. Introduction

Currently, massive rotator cuff tears (MRCTs) remain a therapeutic challenge because of the inability to achieve complete repair in some cases and the higher postoperative retear rates.[1–4] The main reasons for the high retear rates are believed to be due to higher repair tension and

* Corresponding author. Department of Sports Medicine, Huashan Hospital, Fudan University, No. 12 Urumq Middle Road, Shanghai, 200040, China.
** Corresponding author. Department of Sports Medicine, Huashan Hospital, Fudan University, No. 12 Urumq Middle Road, Shanghai, 200040, China.
E-mail addresses: biochenjun@fudan.edu.cn (J. Chen), hua_cosm@aliyun.com (Y. Hua).
[1] Yuyan Na, Hao Jue, and Tian Xia contributed equally to this work.

https://doi.org/10.1016/j.asmart.2024.01.007
Received 13 November 2023; Accepted 17 January 2024

the failure of fibrocartilage regeneration at the tendon-to-bone junction.[5,6] Chronic muscle degeneration and tear size in the mediolateral direction are strongly associated with repairing tension.[6] During the tendon-to-bone healing process, fibrovascular scar tissue forms, which is characterized by disorganized collagen fibrils and proliferating blood vessels and is responsible for poor mechanical properties.[7] Therefore, the key to reducing the postoperative retear rate lies in effectively minimizing tension at the repair site and promoting fibrocartilage regeneration.

Numerous procedures have been investigated to repair MRCTs. These procedures include arthroscopic debridement, partial cuff repair, tendon transfer, superior capsular reconstruction, subacromial spacer interposition, and reverse total shoulder arthroplasty.[8–14] While most of these techniques aim to restore force-couple balance and have acceptable clinical results, none of them provide anatomical repairs.

Bridging repair is one of the treatment options for MRCTs.[15,16] The principal purpose of bridging repair is to interpose a graft between the torn tendon and the footprint, followed by suturing.[16] Bridging repair is an anatomical repair. This technique reduces the tension of the repaired tendon and preserves the contractile function of the muscle. When compared to other techniques that require grafts, such as superior capsule reconstruction and augmentation repair, the bridging technique offers several advantages.[15–17] In a systematic review comparing bridging repair with superior capsular reconstruction for MRCTs, it was found that bridging repair resulted in significantly better shoulder function scores (measured by Constant-Murley score and American Shoulder and Elbow Surgeons score), visual analog scale pain scores, and active external rotation mobility.[16] Another review comparing clinical outcomes of bridging versus augmentation repair of MRCTs showed overall healing rates of 77.9% and 64.0%, respectively, with the bridging group showing more significant improvement in pain during the follow-up period.[17] Therefore, the bridging repair technique is a viable option for the clinical treatment of MRCTs.

Since the initial bridging with a freeze-dried cuff allograft in 1978, alternative types of grafts have been proposed and used for bridging reconstruction. These grafts include fascia lata (FL) autograft, dermal allograft or xenograft, and synthetic patches.[18–22] Although these grafts have been used for bridging repairs with improved clinical outcomes, there is no evidence as to which graft provides the better repair results.[19–21] Additionally, there is a lack of animal studies comparing bridging repairs of MRCTs with these grafts.

Therefore, in this study, we utilized clinically used grafts (autologous FL, acellular dermal matrix graft (ADM), and polyethylene terephthalate (PET) patch) for bridging repairs in a chronic MRCTs rabbit model. The healing process of these grafts was evaluated and compared histologically and biomechanically at 6 and 12 weeks postoperatively. These findings have the potential to provide clear evidence on the efficacy of each graft for the treatment of MRCTs.

2. Material and methods

2.1. Characterization of grafts

The micromorphology of the grafts was observed using scanning electron microscopy (Hitachi SU8010, Japan) at an accelerating voltage of 20 kV after being vacuum-coated with gold. Following this, a mechanics test was performed on each graft. Samples were cut into rectangles (0.4 cm wide and 5 cm long) and were immersed in saline for 5 min prior to testing. To ensure that maximum failure load and elastic modulus were comparable, the initial distance between clamps was set to 1 cm. After preconditioning, the test began with an elongation rate of 5 mm/min in the vertical plane, and the load-deformation curve was recorded.

2.2. Animal study

The animal experimental protocol was approved by the Institutional Animal Care and Use Committee. This work has been reported in accordance with the ARRIVE guidelines (Animals in Research: Reporting In Vivo Experiments).[23] The animal experimental process was illustrated in Fig. 1. Sixty-six male New Zealand White Rabbits, aged 16 weeks and weighing 3.0 ± 0.2 kg, were chosen for this study. To mimic chronic rotator cuff tears in humans, a rabbit model of chronic MRCTs was created. The rabbits were anesthetized with Zoletil 50 (a mixture of tiletamine and zolazepam) at a dosage of 0.3 ml/kg through intramuscular injection. Once the anesthesia was deemed satisfactory, the shoulder was shaved and sterilized. A longitudinal incision of approximately 3 cm was made on the right shoulder, exposing the infraspinatus tendon that was covered by a layer of the deltoid muscle. The deltoid muscle was incised, the infraspinatus tendon was completely detached from the footprint using a scalpel blade, and the fibrocartilage in the footprint was thoroughly removed. To establish an irreparable MRCTs model, the infraspinatus tendon was shortened by 8 mm, ensuring that the stump could not return to the footprint. The stump was marked with a No. 4-0 Ethibond (Ethicon) suture, and the muscle, fascia, and skin were sutured layer by layer. Postoperatively, the rabbits received a continuous intramuscular injection of 40,000 U of penicillin G once daily for three days to prevent infection.

Study has demonstrated that there is significant muscle degeneration, including muscle atrophy and muscle fat infiltration, in the rotator cuff muscles of rabbits six weeks after tenotomy.[24] After the six-week modeling period, the infraspinatus muscles of three rabbits in the tenotomy group, as well as the infraspinatus muscles of three normal rabbits, were harvested. Bilateral muscle wet weight was measured to calculate the muscle atrophy ratio on the surgical side (right side): (IS (right) - IS (left)) ÷ IS (left). Subsequently, the right infraspinatus muscles were frozen and stained with oil red to observe muscle fat infiltration. The remaining 60 rabbits underwent secondary surgery for bridging repair of MRCTs. In the FL group, FL strip of 20 mm × 4 mm was harvested through a 4 cm longitudinal incision on the proximal-lateral side of the ipsilateral thigh and was folded in half to double its thickness. The size of the three grafts was standardized to 10 × 4 mm (Fig. 2 A, C, E).

Bridging reconstruction was performed 6 weeks after the cuff defect was created. After adequate anesthesia, a longitudinal incision was made along the original incision site in the right shoulder, revealing the infraspinatus tendon with caution. It was observed that the fibrovascular scar tissue had reattached to the footprint. The marked sutures were used as a guide to completely remove the scar tissue, while a scalpel blade was employed to remove the fibrocartilage in the footprint again. Two parallel bone tunnels were drilled with 1.0 mm K-wire at the original infraspinatus tendon insertion posteriorly to the lateral cortical bone of the greater tuberosity. The grafts were sutured to the stump of tendon using 2 mattress sutures with No. 2-0 Ethibond suture, and the lateral edge of the grafts was fixed to the footprint of the greater tuberosity in a transosseous fashion by passing a No. 2-0 Ethibond suture (Fig. 2B–D, F).[25] The rabbits were not immobilized postoperatively. For infection prophylaxis, 40,000 U of penicillin G was administered intramuscularly once a day for three consecutive days.

2.3. Histological analysis

Frozen infraspinatus muscle was taken 6 weeks after tenotomy for oil red staining. At 6 and 12 weeks postoperatively, rabbits from each group were euthanized and tissue samples were harvested for histological analysis. After removing the soft tissues and capsule, the infraspinatus tendon–humerus complexes were kept intact. Histologic observation was divided into three sections: the graft-to-tendon junction, the tendon substance, and the graft-to-bone junction. Specimens were fixed in 4% paraformaldehyde for 24 h, and the complexes were decalcified with

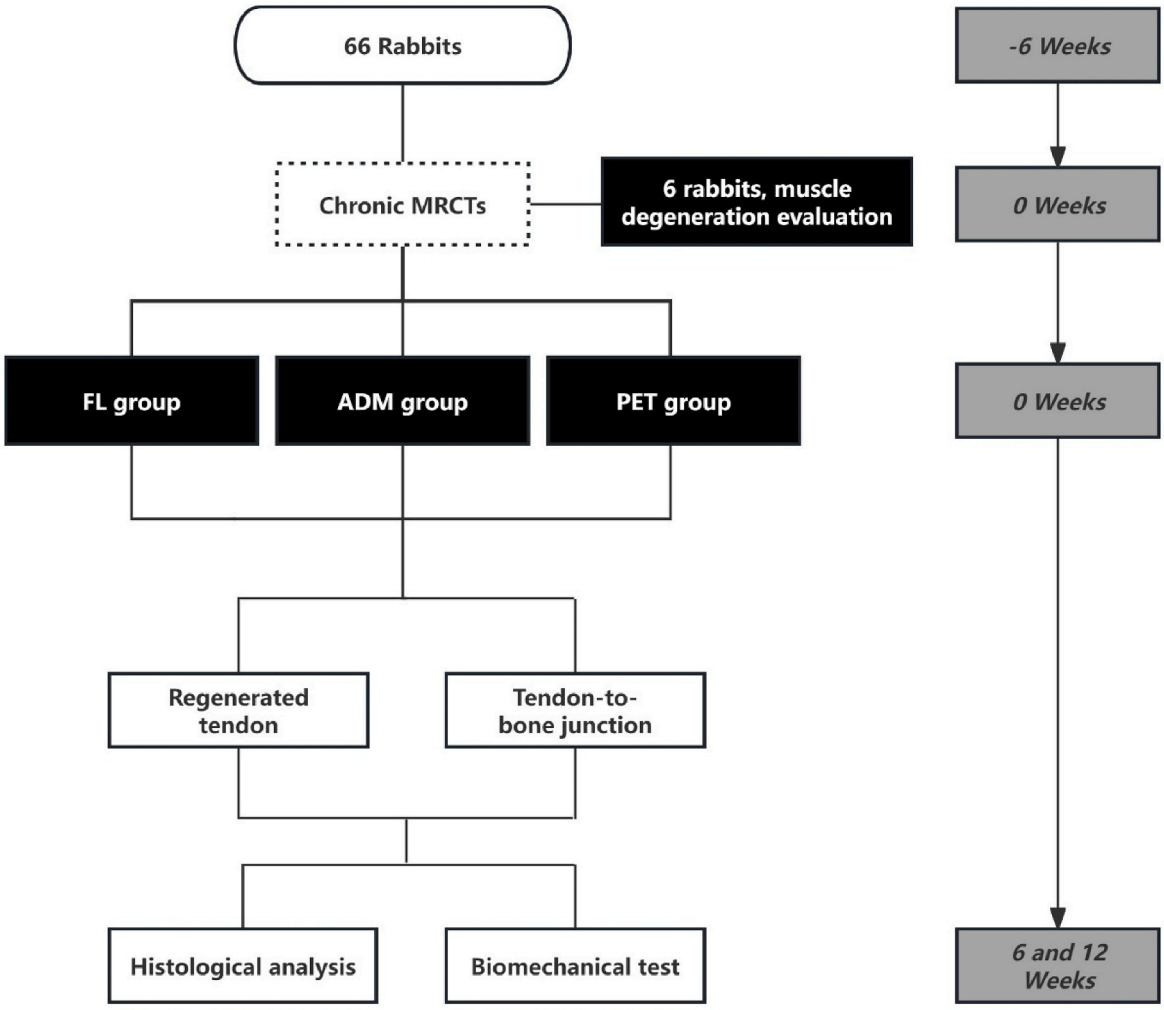

Fig. 1. The animal experimental process. FL, fascia lata; ADM, acellular dermal matrix; PET, polyethylene terephthalate; MRCTs, massive rotator cuff tears.

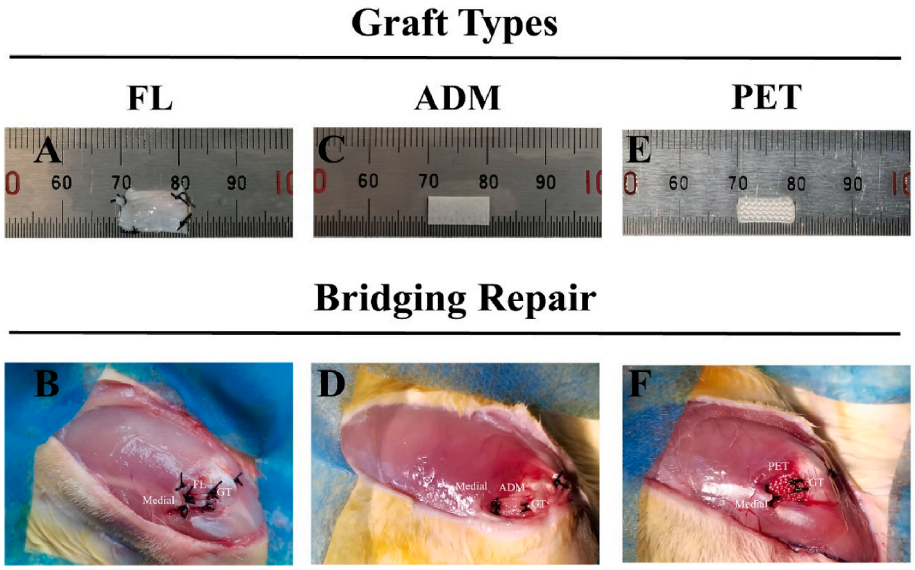

Fig. 2. A schematic diagram of bridging repair techniques using different grafts. After the (A) FL autograft, (C) ADM xenograft, (E) PET synthetic patch was prepared, bridging repairs were performed in a chronic, MRCTs model in rabbits. (B) Completion of bridging repair with FL. (D) Completion of bridging repair with ADM. (F) Completion of bridging repair with PET. FL, fascia lata; ADM, acellular dermal matrix; PET, polyethylene terephthalate; MRCTs, massive rotator cuff tears.

10% EDTA for 4–6 weeks. After dehydration, the complexes were processed for paraffin embedding, and continuous sections (4 μm thick) were cut along the long axis of the infraspinatus tendon and through the transverse plane of the graft-to-bone junction. The sections were then stained with Hematoxylin and eosin (HE) to characterize the morphology. The Modified Tendon Histological Evaluation (MTHE) score was used to semiquantitatively evaluate maturity of the regenerated tendon (Appendix Table 1).[26,27] For semiquantitative evaluation of tendon-to-bone healing, the histologic scoring system described by Jang et al. was used (Appendix Table 2).[25,28] Picrosirius red staining images were captured using a polarized light microscope (Nikon Eclipse E800, Japan) to analyze the type I and III collagen content as a percentage of the pixels.[29] In addition, the sections were stained with Safranin O/Fast green staining to semiquantitatively assess the regenerated fibrocartilage metachromasia ratio. These semiquantitative analysis were performed with Image J software (National Institutes of Health) by 2 independent observers.

Immunohistochemistry analysis was used to detect the expression of osteopontin (OPN) at the tendon-to-bone interface at 6 and 12 weeks after surgery. The sections were incubated with anti-OPN primary antibody (ab214050; Abcam) overnight at 4 °C, followed by incubation with secondary antibody for 1 h at 37 °C. After DAB chromogenic reaction and nucleus counterstaining in hematoxylin, the sections were dehydrated and mounted. Immunofluorescence analysis was also performed to detect macrophage infiltration in the tendon substance using anti-CD68 antibody (ab955; Abcam) after punching with 0.1% TritonX-100 and blocking with 5% BSA. DAPI staining and mounting with a fluorescence quencher were conducted. Average optical density of immunohistochemical analysis against OPN or CD68-positive cell counting was quantified by ImageJ software.

2.4. Transmission electron microscopy (TEM) evaluation

The distribution of regenerated collagen fibrils in the tendon substance at 6 and 12 weeks after surgery was analyzed with TEM. The regenerated tendon, measuring 1 mm^3, was fixed in 2.5% glutaraldehyde for 24 h at 4 °C. The fixed sample was dehydrated with an increasing ethanol gradient and filtrated in transparent resin. After slicing, the sample was transferred onto a copper grid and observed under TEM (Hitachi HT7800, Japan). The diameter distribution of regenerated collagen fibrils was determined using ImageJ software and Origin 2021, with a minimum of 500 fibrils measured in each sample. To assess fibril density, fibril count was conducted in one square micrometer of each sample.

2.5. Biomechanical testing

The maximal failure load and elastic modulus of the fresh infraspinatus tendon–humerus complexes were tested by an electronic universal testing machine (UTM4304, SUNS, China) at 6 and 12 weeks after surgery. The humeral shaft was firmly secured and protected within a polyvinyl chloride tube filled with hardened denture powder, while the proximal infraspinatus was wrapped and protected with medical gauze.[26,30] Before tensile test, the complexes underwent a static preload of 1 N at a rate of 5 mm/min for 20 cycles. Subsequently, an ultimate failure load test was carried out in the vertical plane at an elongation rate of 5 mm/min, and the load-deformation curve was recorded. The test was completed when the curve experienced a sudden, significant drop, indicating the occurrence of a micro-rupture in the complexes.

2.6. Statistical analysis

The sample size calculation for this study was conducted prior to the investigation, using previous reports with an α value of 0.05 and a power (1-β) of 0.8.[25] Based on previous biomechanical data on infraspinatus tendon bridging repair in rabbits, it was determined that a minimum of 5 rabbits per group would be necessary to detect a statistical difference in maximal failure load between the groups. Results are presented as mean ± standard deviation, and statistical analysis was performed using one-way analysis of variance with post-hoc tests. SPSS software (Version 21; IBM) was used for data analysis, and significance was set at $P < 0.05$.

3. Results

3.1. Characterization of grafts

Surface micromorphology of grafts was observed via scanning electron microscopy. Knitted fibers of PET patch exhibited aligned distribution, while the random orientation was observed in FL and ADM (Fig. 3A). As shown in Fig. 3C, the maximal failure load of PET (428.3 ± 2.89 N) was significantly higher than that of FL (48.74 ± 3.04 N) and ADM (42.31 ± 2.01 N) ($P < 0.0001$). Meanwhile, the elastic modulus of FL (122.2 ± 2.48 MPa) and PET (428.9 ± 3.40 MPa) were significantly higher than that of ADM (61.80 ± 2.80 MPa) ($P < 0.0001$) (Fig. 3D).

3.2. Establishment of the chronic MRCTs model and gross observations of tendon-bone complex

Chronic MRCTs are commonly accompanied by muscle degeneration, such as muscle atrophy and fatty infiltration. Compared to normal muscle, a significant loss of muscle weight was observed at 6 weeks after tenotomy ($P = 0.012$) (Fig. 4A). Additionally, oil red staining indicated a significant increase in fat infiltration within the muscle at 6 weeks post-tenotomy, compared to the normal group ($P = 0.027$) (Fig. 4B and C). These results collectively demonstrate the successful establishment of the rabbit model for the chronic MRCTs.

Postoperative observation of specimens revealed no graft ruptures, infections, or defects at the graft-bone junction in all groups (Fig. 4D). The normal infraspinatus tendon gradually become smoother and narrower from the proximal to distal regions. And the white tendon at the tendon-bone junction was clearly visible. At 12 weeks after repair, there was a significant amount of hyperplastic synovium surrounding the tendon-bone junction in all three groups, and the overall morphology of the regenerated tendon was slightly wider and thicker compared to the normal tendon.

3.3. Histological and immunostaining assay

3.3.1. Regenerated tendon

At 6 weeks postoperatively, three groups showed hypercellularity at the regenerated tendon with moderately disordered distribution of round and spindle-shaped nuclei. Regenerated collagen fibers were highly dense and moderately well-ordered in the three groups (Fig. 5A and B). Magnified photographs of tenocytes morphology and blood vessels were shown in the Appendix Fig. 1. Simultaneously, large amounts of regenerated collagen were detected within the PET patch. Notably, the MTHE score was significantly higher in the FL group than in the PET group at this time (13.2 ± 1.64 vs 9.6 ± 1.95, respectively; P = 0.038) (Fig. 5D). Under polarized light microscopy, the results of picrosirius red staining exhibited a differential distribution of type I and III collagen fibers within the regenerated tendons (Fig. 5C). Specifically, percentage of type I collagen (represented by yellow pixels) was markedly higher in the FL group compared to the ADM and PET groups (0.754 ± 0.034 vs 0.623 ± 0.026 vs 0.583 ± 0.095, respectively, $P < 0.05$) (Fig. 5E). Meanwhile, percentage of type III collagen (represented by green pixels) in the FL group was significantly lower than that detected in the ADM group (0.067 ± 0.028 vs 0.136 ± 0.051, respectively, $P = 0.036$) (Fig. 5F). Macrophage infiltration was significantly greater in the ADM and PET groups compared to the FL group (12.550 ± 3.792% vs 14.250 ± 5.377% vs 5.871 ± 1.831%, respectively, $P < 0.05$) (Fig. 6B). In the ADM group, macrophages were clustered within the degraded matrix, while in the PET group, macrophages mainly encircled the

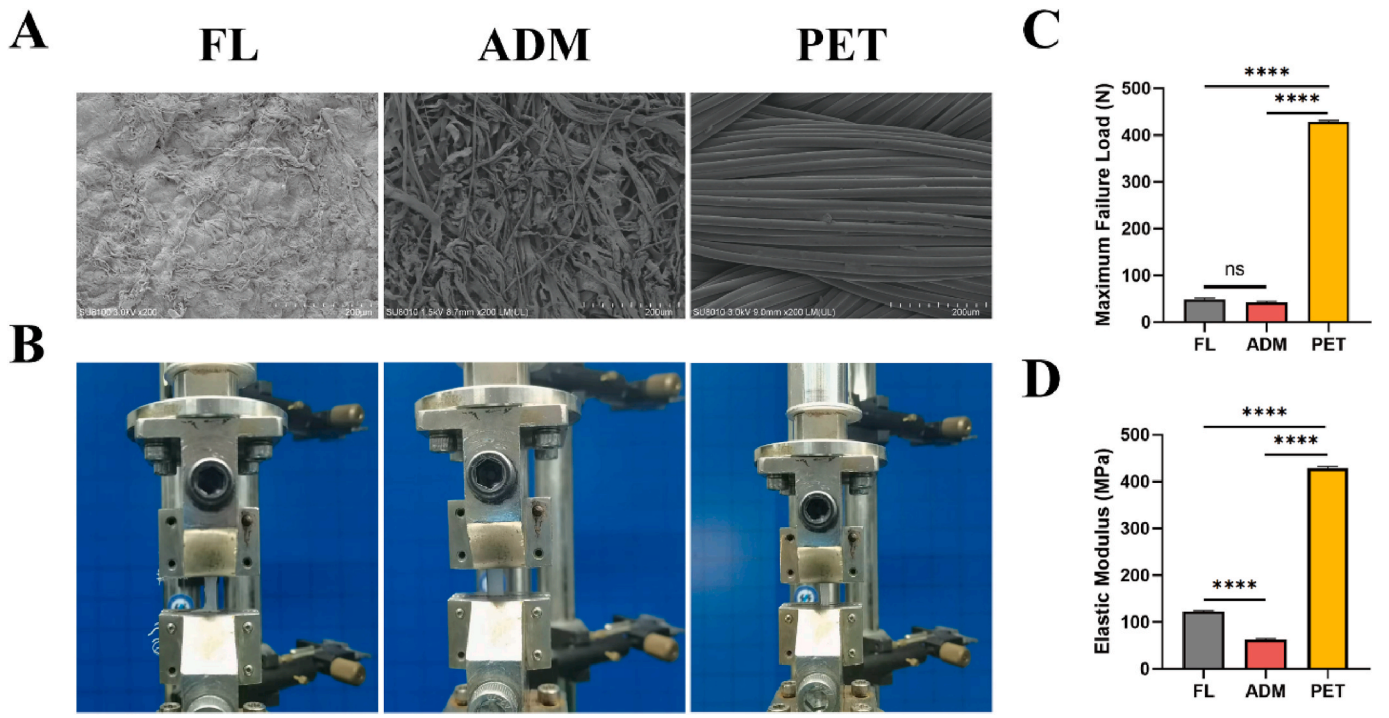

Fig. 3. Micromorphology and mechanical properties of the three grafts. (A) SEM morphology, (B) Image of biomechanical test. Comparison of the maximal failure load (C) and the elastic modulus (D) between the grafts. Ns: no significance. ****$P < 0.0001$. FL, fascia lata; ADM, acellular dermal matrix; PET, polyethylene terephthalate.

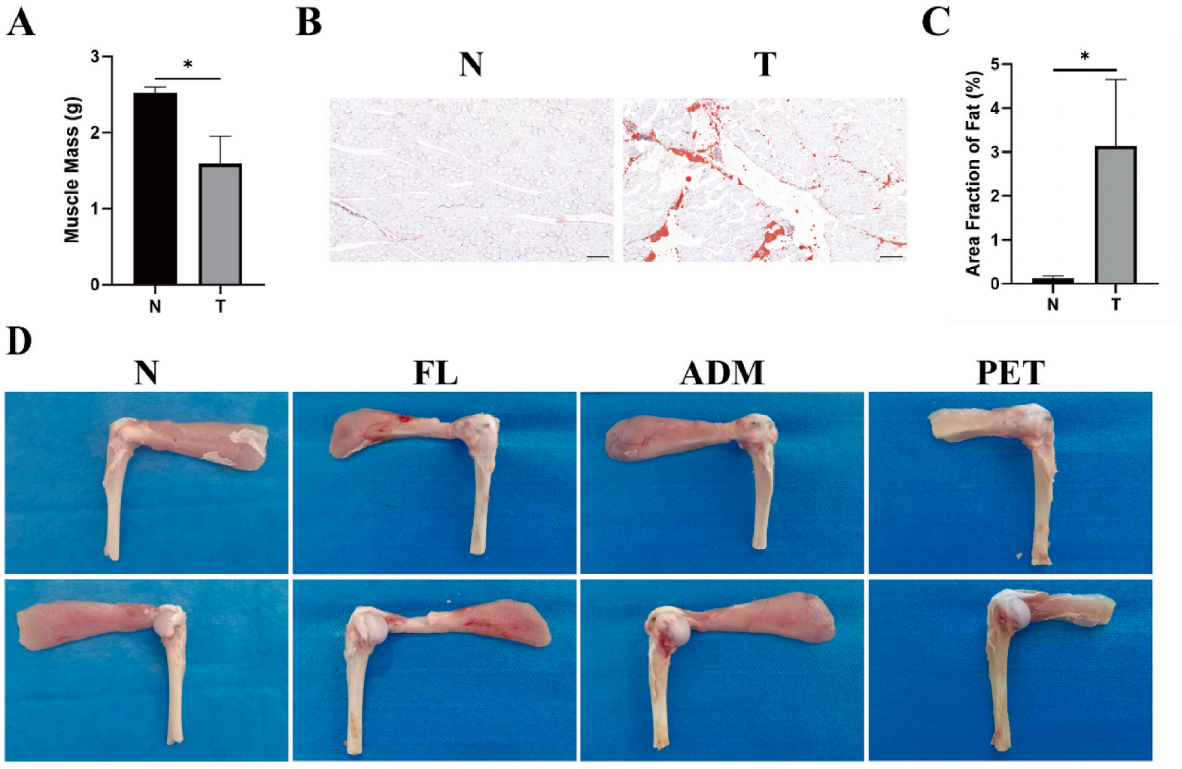

Fig. 4. Muscle degeneration of the chronic MRCTs model and gross observation of the tendon-bone complex. (A) Muscle mass, (B) Oil Red O staining, the black scale bar equals 200 μm, (C) The ratio of the fat area. (D) Gross evaluation in bursal and articular sides of the tendon-bone complex at 12 weeks after repair. *$P < 0.05$. N, normal; T, tenotomy; FL, fascia lata; ADM, acellular dermal matrix; PET, polyethylene terephthalate.

surface and interior of the patch.

At 12 weeks postoperatively, the regenerated tendon showed cell and blood vessel densities comparable to healthy tissue in the three groups, with tenocyte nuclei were long spindle-shaped, and sometimes arranged in rows. And more compact and parallel regenerated collagen fibers were found (Fig. 5A and B). No significant difference in the MTHE

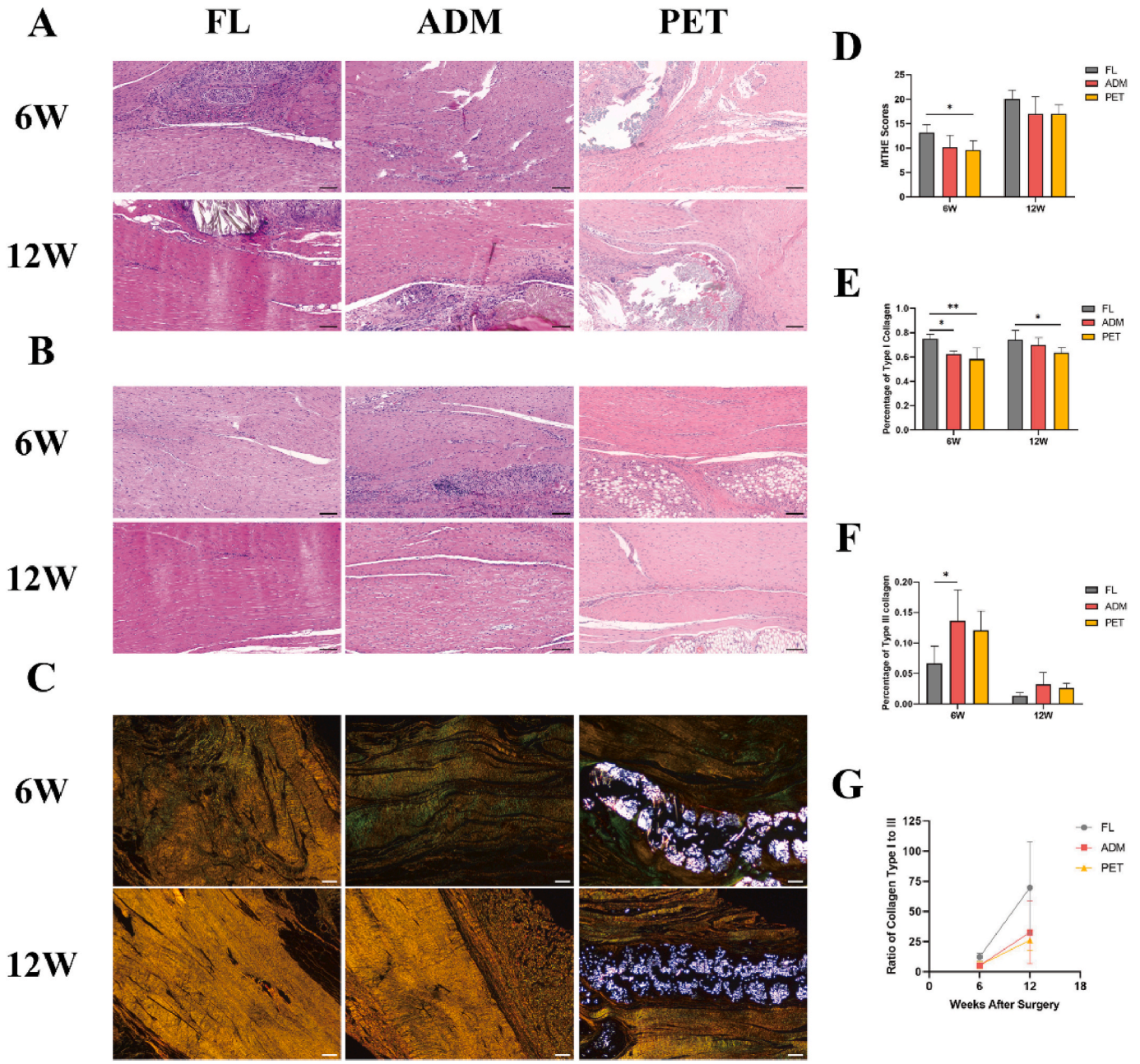

Fig. 5. Histological analysis of the regenerated tendon. Hematoxylin-eosin staining images of the graft-to-tendon junction (A) and the regenerated tendon substance (B) in the FL, ADM, and PET groups at 6W and 12W. The black scale bar equals 100 μm. (C) Picrosirius red staining images of the regenerated tendon in the FL, ADM, and PET groups at 6W and 12W. The white scale bar equals 200 μm. (D) The MTHE scores for the regenerated tendon. (E) Percentage of type I collagen (a percentage of the yellow pixels of each image) of the regenerated tendon in picrosirius red staining. (F) Percentage of type III collagen (a percentage of the green pixels of each image) of the regenerated tendon in picrosirius red staining. (G) Ratio of type I collagen to type III collagen at 6W and 12W after surgery. *$P < 0.05$. **$P < 0.01$. W, weeks; FL, fascia lata; ADM, acellular dermal matrix; PET, polyethylene terephthalate; MTHE, Modified Tendon Histological Evaluation.

score was observed between the experimental groups (Fig. 5D). Picrosirius red staining revealed a significant increase in type I collagen content and a marked decrease in type III collagen content among the experimental groups, suggesting a substantial substitution of type III collagen with type I collagen during tendon regeneration over time (Fig. 5G). Notably, percentage of type I collagen remained significantly higher in the FL group compared to the PET group (0.744 ± 0.076 vs 0.637 ± 0.041, respectively, $P = 0.04$) (Fig. 5E). While macrophage infiltration was significantly reduced in the ADM and PET groups compared to previous levels, it remained higher than that observed in the FL group (8.856 ± 1.196% vs 8.569 ± 2.883% vs 2.590 ± 0.967%, respectively, $P < 0.01$) (Fig. 6C).

3.3.2. *Tendon-to-bone junction*

At 6 weeks post-operation, HE staining showed that the regenerated infraspinatus tendon had successfully reattached to the footprint in all experimental groups. (Fig. 7A). There was a moderately disorganized arrangement of numerous inflammatory and tendon cells present at the tendon-to-bone interface, with no obvious fibrocartilage regeneration and rare sharpey-like fibers. Interface tissue transition from tendon to bone was clear. The metachromasia area of Safranin O exhibited no significant difference between the experimental groups (Fig. 7E), and no significant difference in the histological score of tendon-to-bone healing was observed (Fig. 7D). Furthermore, there was no notable difference in the expression of OPN observed on the immunohistochemical images of

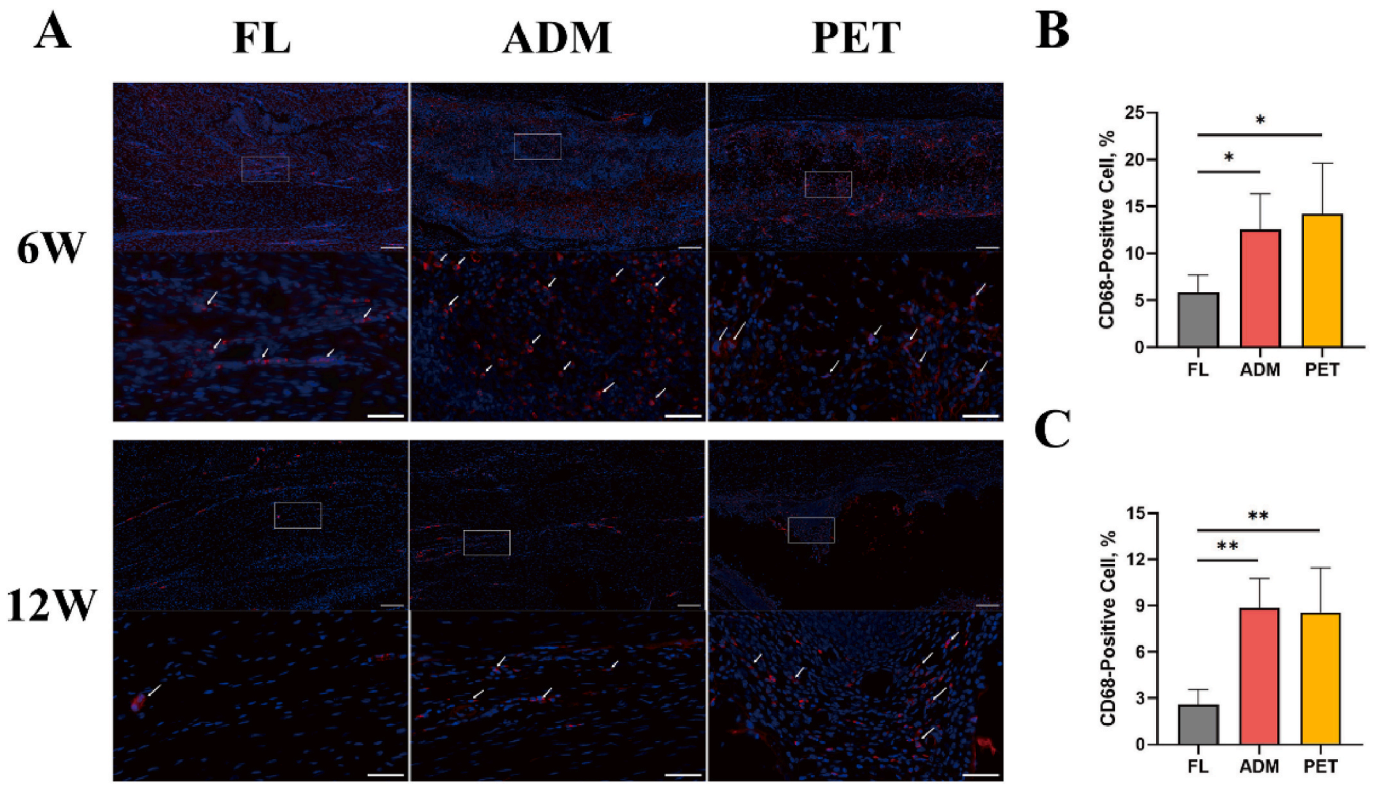

Fig. 6. Immunofluorescence analysis against CD68 of the regenerated tendon substance. (A) The representative image of CD68 expression of the regenerated tendon substance among the experimental groups at 6W and 12W. The white arrow indicates infiltrated macrophages. The scale bar equals 200 μm. The scale bar of the high-magnification images of rectangles equals 50 μm. Quantitative analysis of CD68-positive cell of the regenerated tendon substance among the experimental groups at 6W (B) and 12W (C). *$P < 0.05$. **$P < 0.01$. W, weeks; FL, fascia lata; ADM, acellular dermal matrix; PET, polyethylene terephthalate.

the experimental groups (Fig. 7C–F).

At 12 weeks after repair, regenerated fibrocartilage could be observed at the interface in some views (Fig. 7B). Sharpey-like fibers remained scarce. The transition of the interface from tendon to bone was obscured. Regenerated collagen fibers were directly embedded in the bone in some areas. Some PET sections showed sutures and non-resorbable fibers embedded in the bone, which may have an impact on fibrocartilage regeneration. The area of Safranin O metachromasia was significant greater in ADM group than that in the PET group (76748 ± 36248 vs 19019 ± 21772, respectively, $P = 0.01$) (Fig. 7E). No significant difference in the expression of OPN was found on the immunohistochemical images (Fig. 7C–F).

3.4. TEM evaluation

Diameter distribution of the regenerated collagen fibrils in the experimental groups followed a normal distribution (Fig. 8A). The transverse section of fibrils was also quantitatively assessed using collagen diameter and fibrils density. At 6 weeks postoperatively, the collagen diameter of the regenerated tendons was markedly larger in the FL group compared to the PET group (42.57 ± 2.33 nm vs 38.28 ± 2.18 nm, respectively, $P = 0.043$). Moreover, the collagen diameter of the regenerated tendons in both the FL and ADM groups was significantly larger than that in the PET group at 12 weeks postoperatively (56.45 ± 1.74 nm vs 55.77 ± 4.65 nm vs 48.54 ± 1.42 nm, respectively, $P < 0.05$) (Fig. 8B). However, no difference was observed in the fibrils density in one square micrometer of the regenerated tendons among the experimental groups at 6 and 12 weeks post-operation (Fig. 8C).

3.5. Biomechanical testing

At 6 and 12 weeks after the surgical intervention, the maximal failure load and elastic modulus of the healed tendon-bone complex were measured and compared. Notably, both parameters of the complex improved over time. It is noteworthy that when the load-deformation curve showed a sudden and significant drop, tiny tears were often observed, primarily at the tendon-to-bone interface and the graft-to-tendon junction (Fig. 9B). At 6 weeks postoperatively, the maximum failure load was significantly higher in the FL group compared to the ADM group (118.40 ± 16.70 N vs 93.75 ± 9.06 N, respectively; $P = 0.019$) (Fig. 9C). Furthermore, the elastic modulus was significantly higher in the FL group than in the ADM group at both 6 weeks (12.28 ± 1.94 MPa vs 9.58 ± 0.79 MPa, respectively; $P = 0.024$) and 12 weeks (15.02 ± 2.36 MPa vs 11.63 ± 1.20 MPa, respectively; $P = 0.032$) postoperatively (Fig. 9D).

4. Discussion

This study demonstrated that all three grafts could successfully bridging chronic MRCTs in a rabbit model. However, the FL group exhibited superior results compared to the ADM and PET groups. The regenerated tendons in the FL group displayed higher MTHE scores and type I collagen content, and larger regenerated collagen diameter, while also presenting less macrophage infiltration than those in the ADM and PET groups. Furthermore, biomechanical tests revealed a higher failure load and elastic modulus in the FL group than the ADM group. In addition, at 12 weeks after repair, the ADM group exhibited a statistically significant advantage in terms of fibrocartilage regeneration than the PET group.

FL is a common autograft that has been utilized in hernia repair surgeries.[31,32] However, in rotator cuff surgery, it is more frequently used for superior capsule reconstruction.[33,34] In a study conducted by Hasegawa et al. using FL to reconstruct the superior capsule of MRCTs in rabbits, they found a gradual ligamentous evolution of the graft after

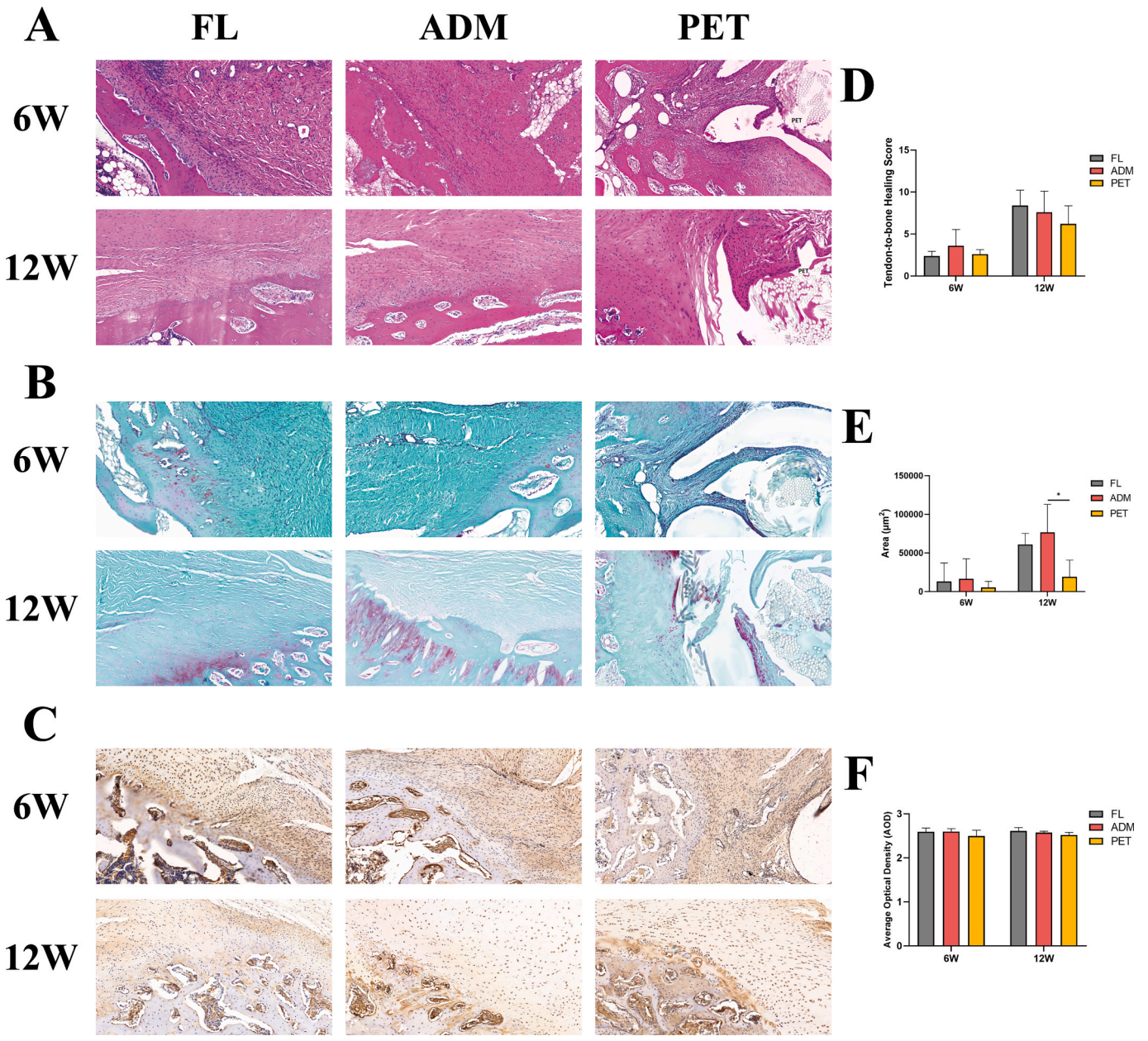

Fig. 7. Morphological features of the tendon-to-bone interface and evaluation of fibrocartilage and bone regeneration. (A) Morphological characteristics of the interface were evaluated by HE staining. The scale bar equals 100 μm. (B) Fibrocartilage regeneration of the interface was assessed by Safranin-O/Fast Green staining. The scale bar equals 100 μm. (C) Immunohistochemical analysis against OPN at the tendon-to-bone interface. The scale bar equals 200 μm. (D) Tendon-to-bone healing histologic score from HE staining in the FL, ADM, and PET groups at 6W and 12W. (E) Quantitative assessment of metachromasia ratio at the interface from Safranin-O/Fast Green staining. (F) Quantitative analysis of average optical density at the interface from immunohistochemical analysis against OPN. *P < 0.05. W, weeks; FL, fascia lata; ADM, acellular dermal matrix; PET, polyethylene terephthalate; HE, Hematoxylin and eosin.

surgery, which encouraged us to use FL for bridging repair.[35] During the bridging repair, the graft was sutured to the tendon stump at one end, which facilitated tendon regeneration. In this study, the maturity of the regenerated tendon (MTHE score) was significantly higher in the FL group compared to the PET group at 6 weeks post-operation. Furthermore, picrosirius red staining revealed a significantly higher type I collagen content in the regenerated tendon of the FL group when compared with the ADM and PET groups. These results are thought to be linked to the number and duration of macrophage infiltration.

The immune response of the body after graft reconstruction is a crucial factor in tissue healing and regeneration, with macrophage infiltration playing a key role.[36] Chronic macrophage infiltration can trigger the formation of fibrotic films through the recruitment of fibroblasts, which can negatively impact graft-organism integration.[37,38] Moreover, chronic macrophage response can cause vascular proliferation within the regenerating tendon, which is a negative indicator of the evolution of tendon maturation.[39] Although ADM and PET have excellent biocompatibility, a higher number of macrophage infiltrates were observed in these groups compared to the FL group, manifesting as concentrated encapsulation around and within the graft. Likewise, the higher number of macrophages accumulating at the tendon-to-bone interface affected tendon-to-bone healing, which could explain the differences in maximal failure load among FL and the other two groups at 6 weeks post-operation.

Additionally, it has been demonstrated that the infiltration and polarization of macrophages also affect osteogenesis. Interestingly, despite

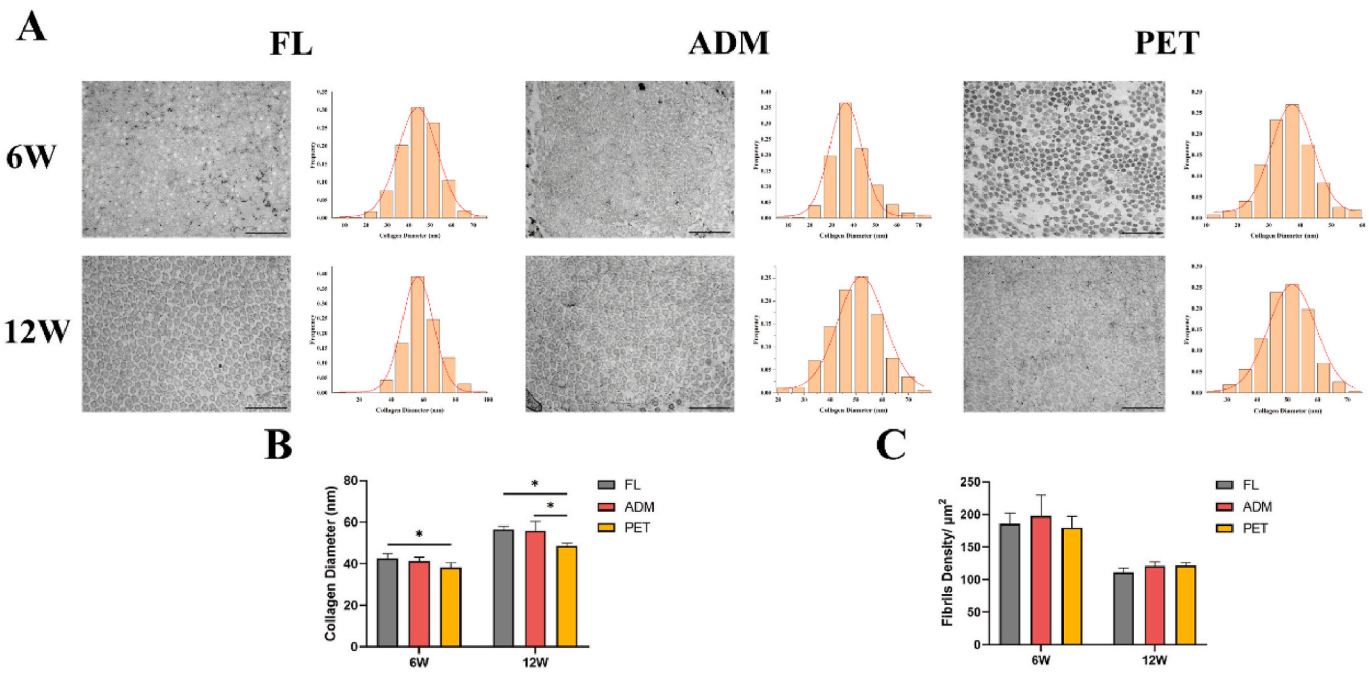

Fig. 8. Microstructural evaluation of the regenerated collagen fibrils. (A) TEM images and diameter distribution of the regenerated collagen fibrils among the experimental groups at 6W and 12W. The scale bar equals 500 nm. Quantitative analysis of collagen diameter (B) and fibrils density (C) at 6W and 12W. *$P < 0.05$. W, weeks; FL, fascia lata; ADM, acellular dermal matrix; PET, polyethylene terephthalate; TEM, transmission electron microscopy.

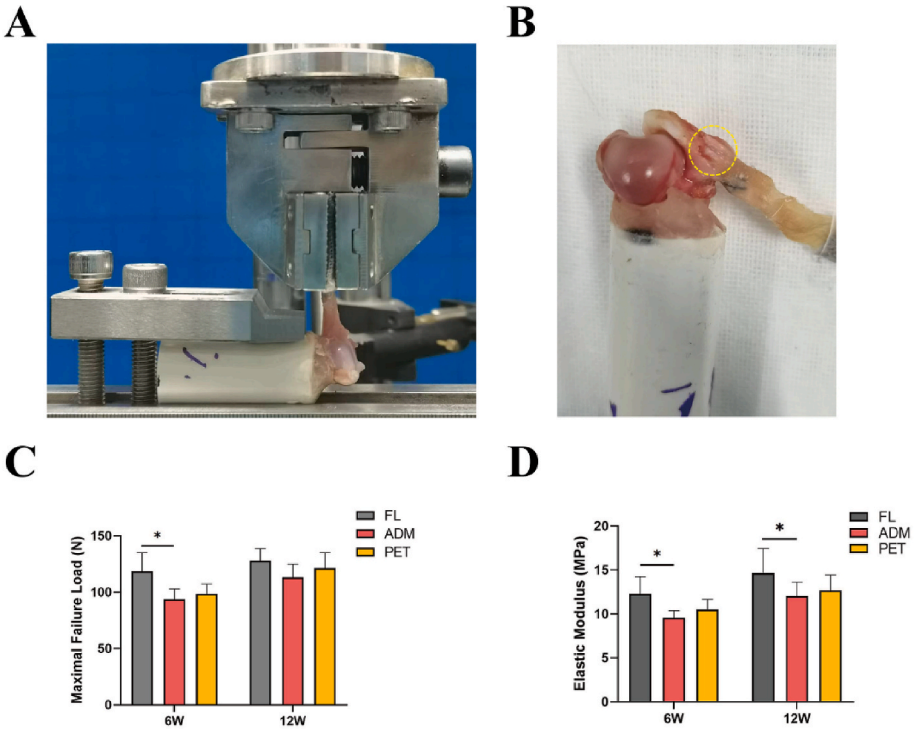

Fig. 9. Results of the biomechanical testing. (A) Mechanical test setting. (B) After biomechanical testing, small tears were identified at the tendon-to-bone junction (indicated by yellow circles). Comparison of the maximal failure load (C) and the elastic modulus (D) among the experimental groups at 6W and 12W. *$P < 0.05$. W, weeks; FL, fascia lata; ADM, acellular dermal matrix; PET, polyethylene terephthalate.

the FL group having the lowest level of macrophage infiltration, it did not show a significant advantage in osteogenesis. This suggested that the complex organismic environment may counteract the effects of macrophage infiltration. It is plausible that these three grafts, which are structurally and functionally simple, have a limited impact on osteogenesis. After anterior cruciate ligament (ACL) reconstruction, it is expected that more regenerated bone would integrate with the grafts, thereby enhancing the overall pull-out strength. While numerous studies have focused on promoting bone regeneration following rotator cuff repair, it is important to prioritize fibrocartilage regeneration over bone regeneration. Excessive bone regeneration, on the other hand, can lead to heterotopic ossification within the tendon and reduce the subacromial

space.The enthesis is a specialized transition area where the tendon/ligament attaches to the bone.[5,40,41] It consists of four distinct layers: ligament/tendon, non-mineralized fibrocartilage, mineralized fibrocartilage, and bone.[7,42] However, fibrocartilage regeneration after rotator cuff repair can be challenging, and the healed interface is often dominated by fibrovascular scar tissue rather than fibrocartilage. This, in turn, greatly reduces the tensile strength and stability of the tendon-to-bone interface.[7,43] In this study, it was observed that at 6 weeks postoperatively, the interface was disorganized with numerous cells and the transition of interface tissue was distinct, with small amounts of fibrocartilage regeneration in the experimental groups. At 12 weeks postoperatively, the area of fibrocartilage regeneration at the tendon-to-bone interface was significantly increased compared with that at 6 weeks. At this time, the metachromasia area of Safranin O was higher in both the FL and ADM groups compared to the PET group. The decellularized dermal and autologous FL contain more native cross-linked structural and matrix components such as collagen, elastin, and proteoglycans, which are also major components of cartilage, and thus may promote fibrocartilage regeneration.[44,45] On the other hand, the synthetic PET is expected to be less biocompatible than the biomaterial, requiring more time for integration with the tissue and regeneration.

Type I collagen is the main component of healthy tendons, while type III collagen is initially produced during the acute phase of tendon injury healing.[29,35] Over time, type III collagen is gradually replaced by type I collagen, which is mechanically stronger due to its aligned orientation and more fibrous cross-links.[46,47] Therefore, the rapid replacement of type III collagen with type I collagen is essential for improving the quality of the regenerated tendon. In this study, picrosirius red staining revealed that at 6 weeks post-operatively, the content of type I collagen in the regenerated tendon was significantly higher in the FL group than in the ADM and PET groups, while the type III collagen content was the lowest. The results indicated that FL graft was the first to achieve type I collagen replacement in the regenerated tendon. This was most directly reflected by the fact that, despite the absence of significant differences in the promotion of fibrocartilage and bone regeneration, the failure load of the tendon-to-bone junction was the highest in the FL group than the ADM and PET groups at this time.

Although the PET patch had a significantly higher failure load and elasticity modulus compared to ADM and FL (as shown in Fig. 3), it did not demonstrate any advantage in the postoperative tendon-bone union biomechanical test. Notably, reliable mechanical strength cannot be immediately attained with PET patch bridging repairs fixed by sutures, as it requires a tendon-to-bone integration process, which differs from the immediate effects of ACL artificial ligament reconstruction.[48] The magnitude of the results of the tendon-to-bone junction biomechanical test after cuff repair depends on the strength of the healing process between the graft and bone, such as fibrocartilage regeneration and increased tendon collagen fibers.[7,49]

The present study has several limitations. Firstly, it is crucial to acknowledge that the anatomy and function of the rabbit shoulder differ from those of humans. For instance, in rabbits, the infraspinatus tendon substance is located directly beneath the acromion, rather than the footprint of the supraspinatus tendon, which necessitated the use of the infraspinatus tendon defect model in this study. Additionally, given that rabbits are limb-walkers and exhibit an accelerated injury healing rate, further controlled clinical trials are indispensable to corroborate the results of this study and ascertain their applicability to human populations. Secondly, while an extended observation period would undoubtedly provide more comprehensive results, it is worth noting that the attainment of tendon-to-bone healing was feasible at 12 weeks post-surgery in the rabbit models.[25,26,27] Thirdly, as each PET and ADM in clinical practice have their own unique properties and processes, it's important to acknowledge that the present results might not fully represent the restorative effects of all similar products.

5. Conclusion

This study demonstrated that all three grafts could successfully bridging MRCTs in a rabbit model. The regenerated tendons in the FL group displayed higher MTHE scores and type I collagen content, and larger regenerated collagen diameter, while also presenting less macrophage infiltration than those in the ADM and PET groups. Furthermore, biomechanical tests revealed a higher failure load and elastic modulus in the FL group than the ADM group. In addition, at 12 weeks after repair, the ADM group showed a statistically significant advantage in terms of fibrocartilage regeneration than the PET group.

Declaration of competing interest

Category 1:Conception and design of study: Yinghui Hua, Jun Chen, Yuyan Na

acquisition of data: Yuyan Na, Hao Jue, Tian Xia

analysis and/or interpretation of data: Yuyan Na, Xiaoao Xue, Luyi Sun.

Category 2: Drafting the manuscript: Yuyan Na

revising the manuscript critically for important intellectual content: Yinghui Hua, Jun Chen.

Category 3: Approval of the version of the manuscript to be published (the names of all authors must be listed): Yuyan Na, Hao Jue, Tian Xia, Xiaoao Xue, Luyi Sun, Jun Chen, Yinghui Hua.

A conflict of interest occurs when an individual's objectivity is potentially compromised by a desire for financial gain, prominence, professional advancement or a successful outcome. *AP-SMART* Editors strive to ensure that what is published in the Journal is as balanced, objective and evidence-based as possible. Since it can be difficult to distin-guish between an actual conflict of interest and a perceived conflict of interest, the Journal requires authors to dis-close all and any potential conflicts of interest.

Section I. The authors whose names are listed immediately below certify that they have NO affiliations with or involvement in any organization or entity with any financial interest (such as honoraria; educational grants; participation in speakers' bureaus; membership, employment, consultancies, stock ownership, or other equity interest; and expert testimony or patent-licensing arrangements), or non-financial interest (such as personal or professional relationships, affiliations, knowledge or beliefs) in the subject matter or materials discussed in this manuscript.

Section II. The authors whose names are listed immediately below report the following details of affiliation or involvement in an organization or entity with a financial or non-financial interest in the subject matter or materials discussed in this manuscript. Please specify the nature of the conflict on a separate sheet of paper if the space below is inadequate.

Acknowledgements

This work was supported by the National Key Research and Development Program of China, Grant Number 2021YFA1201303.

Acknowledgments

All persons who have made substantial contributions to the work reported in the manuscript (e.g., technical help, writ-ing and editing assistance, general support), but who do not meet the criteria for authorship, are named in the Acknowledgements and have given us their written permission to be named. If we have not included an Acknowledgements in our manuscript, then that indicates that we have not received substantial contributions from non-authors.

Appendix

Appendix Table 1
The Modified Tendon Histological Evaluation (MTHE) score for the regenerated tendon substance

Items	Score			
	0	1	2	3
Cell density	Severely increased	Moderately increased	Slightly increased	Normal pattern
Rounding of nuclei	Severely rounded	Moderately rounded	Slightly rounded	Long spindle shape
Cell arrangement	Severely disordered	Moderately disordered	Slightly disordered	Parallel
Fiber density	Severely loose	Moderately loose	Slightly loose	Compacted
Fiber structure	Severely fragmented	Moderately fragmented	Slightly fragmented	Continuous, long fiber
Fiber arrangement	Severely rounded	Moderately rounded	Slightly rounded	Parallel
Inflammation (area infiltrated by inflammatory cells), %	> 30	20–30	10–20	< 10
Increased vascularity, %	> 30	20–30	10–20	< 10
Maximum total score	24			

Appendix Table 2
The histologic scoring of endon-to-bone healing

Items	Score
1. Cellular morphologic characteristics of interface tissue	
Fibrocartilage with mature cartilage cells comprising ≥50%	4
Fibrocartilage with mature cartilage cells comprising <50%	3
Fibrous tissue with Sharpey-like fibers comprising ≥50%	2
Fibrous tissue with Sharpey-like fibers comprising <50%	1
Only fibrovascular tissue	0
2. Extent of surrounding fibrocartilage tissue	
Mostly surrounded (≥75%)	4
Moderately surrounded (50% to < 75%)	3
Partially surrounded (25% to < 50%)	2
Slightly surrounded (<25%)	1
Not visible	0
3. Interface tissue transition from bone to tendon	
Mostly indistinct (≥75%)	4
Moderately indistinct (50% to < 75%)	3
Partially indistinct (25% to < 50%)	2
Continuous but slightly indistinct (<25%)	1
Discontinuous	0
Maximum total score	12

References

1. Haleem A, Gohal C, Leroux T, Henry P, Alolabi B, Khan M. Primary arthroscopic repair of massive rotator cuff tears results in significant improvements with low rate of re-tear. *Knee Surg Sports Traumatol Arthrosc*. 2021;29:2134–2142.
2. Henry P, Wasserstein D, Park S, et al. Arthroscopic repair for chronic massive rotator cuff tears: a systematic review. *Arthroscopy*. 2015;31:2472–2480.
3. Jeong JY, Kim SJ, Yoon TH, Eum KS, Chun YM. Arthroscopic repair of large and massive rotator cuff tears: complete repair with aggressive release compared with partial repair alone at a minimum follow-up of 5 years. *J Bone Joint Surg Am*. 2020; 102:1248–1254.
4. Galatz LM, Ball CM, Teefey SA, Middleton WD, Yamaguchi K. The outcome and repair integrity of completely arthroscopically repaired large and massive rotator cuff tears. *J Bone Joint Surg Am*. 2004;86:219–224.
5. Lei T, Zhang T, Ju W, et al. Biomimetic strategies for tendon/ligament-to-bone interface regeneration. *Bioact Mater*. 2021;6:2491–2510.
6. Takeda Y, Fujii K, Suzue N, Miyatake K, Kawasaki Y, Yokoyama K. Repair tension during arthroscopic rotator cuff repair is correlated with preoperative tendon retraction and postoperative rotator cuff integrity. *Arthroscopy*. 2021;37:2735–2742.
7. Saveh-Shemshaki N, Sn L, Laurencin CT. Nanofiber-based matrices for rotator cuff regenerative engineering. *Acta Biomater*. 2019;94:64–81.
8. Liem D, Lengers N, Dedy N, Poetzl W, Steinbeck J, Marquardt B. Arthroscopic debridement of massive irreparable rotator cuff tears. *Arthroscopy*. 2008;24: 743–748.
9. Berth A, Neumann W, Awiszus F, Pap G. Massive rotator cuff tears: functional outcome after debridement or arthroscopic partial repair. *J Orthop Traumatol*. 2010; 11:13–20.
10. St Pierre P, Millett PJ, Abboud JA, et al. Consensus statement on the treatment of massive irreparable rotator cuff tears: a Delphi approach by the Neer Circle of the American Shoulder and Elbow Surgeons. *J Shoulder Elbow Surg*. 2021;30:1977–1989.
11. Zanini B, Rusconi M, Fornara P, Malgrati F, Grassi FA, Leigheb M. Functional outcome of arthroscopic debridement for massive, irreparable rotator cuff tears. *Acta Biomed*. 2022;92, e2021557.
12. Ozturk BY, Ak S, Gultekin O, Baykus A, Kulduk A. Prospective, randomized evaluation of latissimus dorsi transfer and superior capsular reconstruction in massive, irreparable rotator cuff tears. *J Shoulder Elbow Surg*. 2021;30:1561–1571.
13. Mihata T, Lee TQ, Hasegawa A, et al. Arthroscopic superior capsule reconstruction for irreparable rotator cuff tears: Comparison of clinical outcomes with and without subscapularis tear. *Am J Sports Med*. 2020;48:3429–3438.
14. Hartzler RU, Steen BM, Hussey MM, et al. Reverse shoulder arthroplasty for massive rotator cuff tear: risk factors for poor functional improvement. *J Shoulder Elbow Surg*. 2015;24:1698–1706.
15. Lewington MR, Ferguson DP, Smith TD, Burks R, Coady C, Wong IH. Graft utilization in the bridging reconstruction of irreparable rotator cuff tears: a systematic review. *Am J Sports Med*. 2017;45:3149–3157.
16. Lin J, Sun Y, Chen Q, Liu S, Ding Z, Chen J. Outcome Comparison of graft bridging and superior capsule reconstruction for large to massive rotator cuff tears: a systematic review. *Am J Sports Med*. 2020;48:2828–2838.
17. Ono Y, Dávalos Herrera DA, Woodmass JM, Boorman RS, Thornton GM, Lo IK. Graft augmentation versus bridging for large to massive rotator cuff tears: a systematic review. *Arthroscopy*. 2017;33:673–680.
18. Neviaser JS, Neviaser RJ, Neviaser TJ. The repair of chronic massive ruptures of the rotator cuff of the shoulder by use of a freeze-dried rotator cuff. *J Bone Joint Surg Am*. 1978;60:681–684.
19. Varvitsiotis D, Papaspiliopoulos A, Antipa E, Papacharalampous X, Flevarakis G, Feroussis J. Results of reconstruction of massive irreparable rotator cuff tears using a fascia lata allograft. *Indian J Orthop*. 2015;49:304–311.
20. Neumann JA, Zgonis MH, Rickert KD, et al. Interposition dermal matrix xenografts: a successful alternative to traditional treatment of massive rotator cuff tears. *Am J Sports Med*. 2017;45:1261–1268.

21. Pandey R, Tafazal S, Shyamsundar S, Modi A, Singh HP. Outcome of partial repair of massive rotator cuff tears with and without human tissue allograft bridging repair. *Shoulder Elbow*. 2017;9:23–30.
22. Smolen D, Haffner N, Mittermayr R, Hess F, Sternberg C, Leuzinger J. Application of a new polyester patch in arthroscopic massive rotator cuff repair-a prospective cohort study. *J Shoulder Elbow Surg*. 2020;29:e11–e21.
23. Kilkenny C, Browne WJ, Cuthill IC, Emerson M, Altman DG. Improving bioscience research reporting: the ARRIVE guidelines for reporting animal research. *PLoS Biol*. 2010;8, e1000412.
24. Wang C, Hu Q, Song W, Yu W, He Y. Adipose stem cell-derived exosomes decrease fatty infiltration and enhance rotator cuff healing in a rabbit model of chronic tears. *Am J Sports Med*. 2020;48:1456–1464.
25. Zhong Y, Jin W, Gao H, et al. A knitted PET patch enhances the maturation of regenerated tendons in bridging reconstruction of massive rotator cuff tears in a rabbit model. *Am J Sports Med*. 2023;51:901–911.
26. Xu J, Han K, Ye Z, et al. Biomechanical and histological results of dual-suspensory reconstruction using banded tendon graft to bridge massive rotator cuff tears in a chronic rabbit model. *Am J Sports Med*. 2022;50:2767–2781.
27. Suh DS, Lee JK, Yoo JC, et al. Atelocollagen enhances the healing of rotator cuff tendon in rabbit model. *Am J Sports Med*. 2017;45:2019–2027.
28. Jang KM, Lim HC, Jung WY, Moon SW, Wang JH. Efficacy and safety of human umbilical cord blood-derived mesenchymal stem cells in anterior cruciate ligament reconstruction of a rabbit model: new strategy to enhance tendon graft healing. *Arthroscopy*. 2015;31:1530–1539.
29. Kataoka T, Kokubu T, Muto T, et al. Rotator cuff tear healing process with graft augmentation of fascia lata in a rabbit model. *J Orthop Surg Res*. 2018;13:200.
30. Pulatkan A, Anwar W, Ayık O, et al. Tear completion versus in situ repair for 50% partial-thickness bursal-side rotator cuff tears: a biomechanical and histological study in an animal model. *Am J Sports Med*. 2020;48:1818–1825.
31. Brain RH, Maynard J. Fascia lata graft repair of esophageal hiatal hernia. *Am J Surg*. 1968;115:488–501.
32. Sugiyama A, Fukumoto K, Fukuzawa H, et al. Free fascia lata repair for a second recurrent congenital diaphragmatic hernia. *J Pediatr Surg*. 2011;46:1838–1841.
33. Lee SJ, Min YK. Can inadequate acromiohumeral distance improvement and poor posterior remnant tissue be the predictive factors of re-tear? Preliminary outcomes of arthroscopic superior capsular reconstruction. *Knee Surg Sports Traumatol Arthrosc*. 2018;26:2205–2213.
34. Lim S, AlRamadhan H, Kwak JM, Hong H, Jeon IH. Graft tears after arthroscopic superior capsule reconstruction (ASCR): pattern of failure and its correlation with clinical outcome. *Arch Orthop Trauma Surg*. 2019;139:231–239.
35. Hasegawa A, Mihata T, Itami Y, Fukunishi K, Neo M. Histologic changes during healing with autologous fascia lata graft after superior capsule reconstruction in rabbit model. *J Shoulder Elbow Surg*. 2021;30:2247–2259.
36. Ye J, Xie C, Wang C, et al. Promoting musculoskeletal system soft tissue regeneration by biomaterial-mediated modulation of macrophage polarization. *Bioact Mater*. 2021;6:4096–4109.
37. Brown BN, Ratner BD, Goodman SB, Amar S, Badylak SF. Macrophage polarization: an opportunity for improved outcomes in biomaterials and regenerative medicine. *Biomaterials*. 2012;33:3792–3802.
38. Anderson JM, Rodriguez A, Chang DT. Foreign body reaction to biomaterials. *Semin Immunol*. 2008;20:86–100.
39. Martin P, Gurevich DB. Macrophage regulation of angiogenesis in health and disease. *Semin Cell Dev Biol*. 2021;119:101–110.
40. Calejo I, Costa-Almeida R, Gomes ME. Cellular complexity at the interface: challenges in enthesis tissue engineering. *Adv Exp Med Biol*. 2019;1144:71–90.
41. Benjamin M, Toumi H, Ralphs JR, Bydder G, Best TM, Milz S. Where tendons and ligaments meet bone: attachment sites ('entheses') in relation to exercise and/or mechanical load. *J Anat*. 2006;208:471–490.
42. Apostolakos J, Durant TJ, Dwyer CR, et al. The enthesis: a review of the tendon-to-bone insertion. *Muscles Ligaments Tendons J*. 2014;4:333–342.
43. Li X, Cheng R, Sun Z, et al. Flexible bipolar nanofibrous membranes for improving gradient microstructure in tendon-to-bone healing. *Acta Biomater*. 2017;61:204–216.
44. Ide J, Tokunaga T. Rotator cuff tendon-to-bone healing at 12 months after patch grafting of acellular dermal matrix in an animal model. *J Orthop Sci*. 2018;23:207–212.
45. Adams JE, Zobitz ME, Reach Jr JS, An KN, Steinmann SP. Rotator cuff repair using an acellular dermal matrix graft: an in vivo study in a canine model. *Arthroscopy*. 2006;22:700–709.
46. Xu T, Lin Y, Yu X, et al. Comparative effects of exosomes and ectosomes isolated from adipose-derived mesenchymal stem cells on achilles tendinopathy in a rat model. *Am J Sports Med*. 2022;50:2740–2752.
47. Buckley MR, Evans EB, Matuszewski PE, et al. Distributions of types I, II and III collagen by region in the human supraspinatus tendon. *Connect Tissue Res*. 2013;54:374–379.
48. Fujikawa K, Kobayashi T, Sasazaki Y, Matsumoto H, Seedhom BB. Anterior cruciate ligament reconstruction with the Leeds-Keio artificial ligament. *J Long Term Eff Med Implants*. 2000;10:225–238.
49. Chen W, Sun Y, Gu X, et al. Conditioned medium of human bone marrow-derived stem cells promotes tendon-bone healing of the rotator cuff in a rat model. *Biomaterials*. 2021;271, 120714.